catalysts

MDPI

Article

A Study on the Characteristic and Antibacterial Activity of Ti_3O_x Thin Films

Endrika Widyastuti [1,2], Fu-Yang Xu [3], Chen-Tien Chiu [4], Jhen-Hau Jan [5], Jue-Liang Hsu [6] and Ying-Chieh Lee [3,*]

1 Department of Tropical Agriculture and International Cooperation, National Pingtung University of Science & Technology, Pingtung 91201, Taiwan; endrika_w@ub.ac.id
2 Department of Agricultural Product Technology, Faculty of Agricultural Technology, Universitas Brawijaya, Malang 65145, Indonesia
3 Department of Materials Engineering, National Pingtung University of Science & Technology, Pingtung 91201, Taiwan; young74492@gmail.com
4 Kaohsiung Veterans General Hospital, Kaohsiung City 813414, Taiwan; ctchiu9393@vghks.gov.tw
5 Institute of Materials Science and Engineering, National Central University, Zhongli 32001, Taiwan; jhau.jan@gmail.com
6 Department of Biological Science and Technology, National Pingtung University of Science & Technology, Pingtung 91201, Taiwan; jlhsu@mail.npust.edu.tw
* Correspondence: YCLee@mail.npust.edu.tw

Abstract: A pure Ti target in Ar/O_2 gas mixture was used to synthesize Ti_3O_x thin film on a glass substrate by Reactive High-Power Impulse Magnetron Sputtering (HiPIMS) under different sputtering power (2 and 2.5 kW). The influence of HiPIMS parameters on thin films' structural, morphological, chemical composition, optical and photocatalytic, and antibacterial properties was investigated. In this study, Ti_3O_x thin films can be synthesized using the HiPIMS method without the post-annealing process. Two co-existence phases (hexagonal Ti_3O and base-centered monoclinic Ti_3O_5 phases) existed on the Ti_3O_x films. It is found that the peak intensity of (006) Ti_3O hexagonal slightly increased as the sputtering power increased from 2 to 2.5 kW. The Ti_3O_x thin-film bandgap values were 3.36 and 3.50 eV for 2 and 2.5 kW, respectively. The Ti_3O_x films deposited at 2.5 kW showed good photocatalytic activity under UV light irradiation, with a higher methylene blue dye degradation rate than TiO_2 thin films. The antibacterial study on Ti_3O_x thin films exhibited a high inhibition percentage against *E. coli* and *S. aureus*. This study demonstrates that Ti_3O_x thin films can promote high photocatalytic and antibacterial activity.

Keywords: Ti_3O; Ti_3O_5; Magnéli-phase; *E. coli*; *S. aureus*; reactive-HiPIMS

check for updates

Citation: Widyastuti, E.; Xu, F.-Y.; Chiu, C.-T.; Jan, J.-H.; Hsu, J.-L.; Lee, Y.-C. A Study on the Characteristic and Antibacterial Activity of Ti_3O_x Thin Films. *Catalysts* **2021**, *11*, 1416. https://doi.org/10.3390/catal11111416

Academic Editor: Abel Santos

Received: 30 October 2021
Accepted: 21 November 2021
Published: 22 November 2021

1. Introduction

Titanium sub-oxides (TSO) have drawn much attention as they possess interesting properties for metal oxide thin films which have a variety of crystalline structures; unique physical properties; and a wide range of electrical, optical, and electrochemical properties such as electro-optical devices [1], self-cleaning [2], solar cell [3], and photocatalyst [4]. Magnéli-phase titanium oxides, the Ti_nO_{2n-1}, ($3 \leq n \leq 10$) exhibit specific oxygen vacancies organization that garnered substantial interest owing to their excellent electric conductivity, high corrosion resistance, and optical properties [5,6]. According to Xu et al. [7], Magnéli-phase on TSO is a mixed-valence molecule composed of two Ti^{3+} ($3d^1$ electronic configuration) and (n—2)Ti^{4+} ($3d^0$) ions. The existence of both Ti^{3+} and Ti^{4+} ions in the crystal opens up several possible cation configurations, resulting in a variety of charge-ordered states.

Titanium sub-oxides can be grown by a series of methods, including low-energy ion bombardment [8], pulsed layer deposition [9,10], a chemical vapor deposition (CVD) method [11], sol–gel combined with the energy-efficient vacuum-carbothermic (SF-VC)

process [6], and a sputtering method [12–14]. Among all the deposition techniques, reactive HiPIMS has the capability to grow titanium sub-oxides thin films with alterable oxidation states such as TiO, Ti_2O_3, Ti_3O_5, and TiO_2 crystals with minor oxygen concentration on TiO_2 thin film [15–17]. Numerous studies have highlighted the favorable impact of reactive HiPIMS on thin-film performance, including denser microstructures, higher hardness, lower surface roughness, high degree of crystallinity, and extended phase stabilities or enhanced surface coverage of complex-shaped substrate [18–20]. The reactive sputtering method is typically characterized by the target's composition, influencing the sputtering yield and secondary electron emission coefficient that vary between Ti metal and TiO_2 films [21]. Moreover, besides the elemental coefficients, deposition condition parameters, such as sputtering power, will influence thin films' structure, composition, and photocatalytic properties [22–25].

The properties of single-crystalline TSO such as Ti_2O, Ti_2O_3, Ti_3O_5, Ti_4O_7, TiO_2, etc., have been studied extensively by a few research groups [26–28]. However, it was reported that multiphase composition ($Ti_{20}O_{39}$, TiO_2, Ti_3O, $Ti_{17}O_{33}$, Ti_5O_9, and Ti_2O) on TiO_2 thin films could promote better photocatalytic activity than single-phase titanium [29]. Mixed phase particles of 30% anatase, 25% Ti_4O_7, and 20% Ti_5O_9 also demonstrated the highest photocatalytic H_2 evolution activity [30]. Instead of photocatalytic activity, TiO_2-containing Magnéli phases such as Ti_4O_7, Ti_3O_5, and Ti_2O_3 was reported can enhance the photocatalytic activity [30,31] and antibacterial properties of Hydroxyapatite (Hap) against *E. coli* bacteria [32,33]. The thin-film characteristic has considerable importance, especially for the photocatalytic and antibacterial performance of TSO.

In this study, we have successfully developed multiphase composition on Ti_3O_x thin films prepared using reactive-HiPIMS without the post-annealing process. Ti_3O_x thin films were composed of both Ti_3O and Ti_3O_5 phases. Ti_3O_5, as one of the Magnéli-phase titanium oxides, has been explored in previous studies as an attractive material for its properties of structural transformation. Ti_3O_5 is shown to have excellent photo-reversibility, photocatalysis, oxygen sensitivity, and low resistance temperature coefficient compared to TiO_2 thin film [34–37]. Nevertheless, limited published work refers to the in-cooperation of Ti_3O and Ti_3O_5 phase properties on thin-film photocatalytic and antibacterial activity. In order to observe the fundamental relations between the mixture phase composition (Ti_3O and Ti_3O_5) on the structural, morphology, optical, photocatalytic, and antibacterial properties of Ti_3O_x films, different deposition parameters (sputtering power 2 and 2.5 kW at a constant oxygen flow) were applied in the thin film's preparation. The described synthesis demonstrates that titanium sub-oxides (Ti_3O_x) thin films having Ti_3O and Ti_3O_5 can be successfully synthesized using reactive-HiPIMS methods. This study explores the multi-phase TSO structure, microstructure, chemical composition, optical, photocatalytic properties, and antibacterial activity on Ti_3O_x thin films.

2. Results and Discussion

2.1. Phase Structure and Microstructure of Ti_3O_x Films

The crystal phase of the Ti_3O_x thin films on the glass substrate was characterized by X-ray diffraction (XRD) analysis. The TiO_2 thin films were used to compare with Ti_3O_x thin films samples. Figure 1 shows the XRD patterns of the Ti_3O_x thin films deposited on a glass substrate without post-annealing process as a function of the sputtering power. The presence of the peaks at $2\theta = 37.78°$, $39.76°$, and $52.30°$ correspond to (006), (113), and (116) plane of hexagonal Ti_3O phase (JCPDS card: 76-1644), respectively. Furthermore, (004) and (113) planes resemble the monoclinic Ti_3O_5 phase (JCPDS card: 72-0519). Nupriyonok et al. [38] reported that Ti_3O and Ti_3O_5 were found through the thermal vacuum treatment of Ti films. It is well known that the two essential variables affecting the crystallization of the film during the sputtering process are the thermal energy generated by the substrate heating and the energy of sputtered particles impinging on the substrate surface [25]. However, in this study, the substrates were not intentionally thermal annealing. The crystallization formed in Ti_3O_x film is observed due to the impinging of energetic sputtered

particles, which are under high sputtering power. However, when Ti_3O_x films were annealed at 550 °C for 3 h, it was found that the Ti_3O/Ti_3O_5 phases were transferred to the rutile TiO_2 phase (JCPDS card: 21-1272).

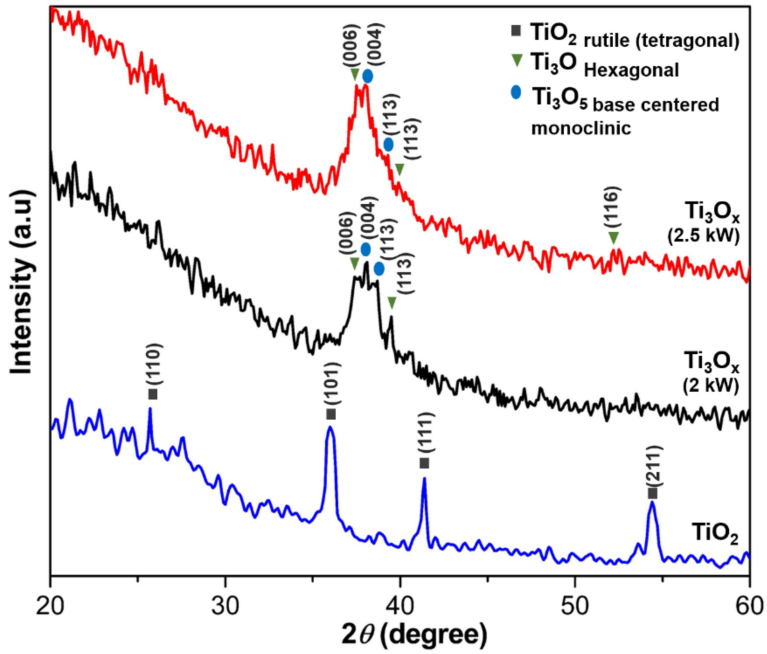

Figure 1. X-ray diffraction pattern of Ti_3O_x thin film deposited at 2 and 2.5 kW. TiO_2 thin films with the related thickness were used as a control.

It was observed that the peak intensity of (006) Ti_3O hexagonal slightly increased as the sputtering power increased from 2 to 2.5 kW. The results indicate that Ti_3O_x films can be prepared using HiPIMS under sputtering power at >2 kW and Ar/O_2 ratio at 200/5 (O_2 ratio: 2.5%). It was reported that Ti_3O_5 is one of the most promising materials for its properties of phase transition photo reversibility, photocatalysis, and oxygen sensitivity [36]. Further study of the microstructure using FE-TEM will be performed to prove this supposition.

The influence of sputtering power on the microstructure of Ti_3O_x as-deposited films was confirmed using High-resolution TEM (HR-TEM). Figure 2a shows the bright cross-sectional field of Ti_3O_x thin film, which is prepared at 2 kW sputtering power. The thickness of the film is approximately 55 nm. The selected zone (inset A) for electron diffraction analysis was used to identify the crystalline phase with a circle area around 200 nm. According to the electron diffraction pattern analysis, the crystalline planes belong to the Ti_3O and Ti_3O_5 phases, as shown in Figure 2b. This observation is consistent with the XRD results, as explained in Figure 1.

Figure 3 exposes the HR-TEM micrographs and selected area diffraction (SAD) pattern of the sample with sputtering power of 2.5 kW. When the sputtering power was enhanced to 2.5 kW, it is obvious that the intensities of the diffraction rings of Ti_3O_X deposited at 2.5 kW were stronger than those 2 kW ones. These results implied that enhancing sputtering to 2.5 kW can promote better crystallinity of Ti_3O_x thin films, as shown in Figure 3a. This finding is also in agreement with XRD analysis (Figure 1) that showed peak intensity of (006) Ti_3O and (004) Ti_3O_5 slightly increased as the sputtering power increased from 2 to 2.5 kW. According to SAD pattern analysis in Figure 3b, the crystalline planes have referred to hexagonal Ti_3O and base-centered monoclinic Ti_3O_5 phases. It found that the increasing sputtering power up to 2.5 kW, drives to the Ti_3O and Ti_3O_5 crystalline intensity increased. Moreover, the intensities of the diffraction rings of (116) Ti_3O plane at 2.5 kW were stronger than at 2 kW. This result is agreed with the XRD analysis (Figure 1) that showed the (116) Ti_3O peak only observed on Ti_3O_x thin film deposited at 2.5 kW.

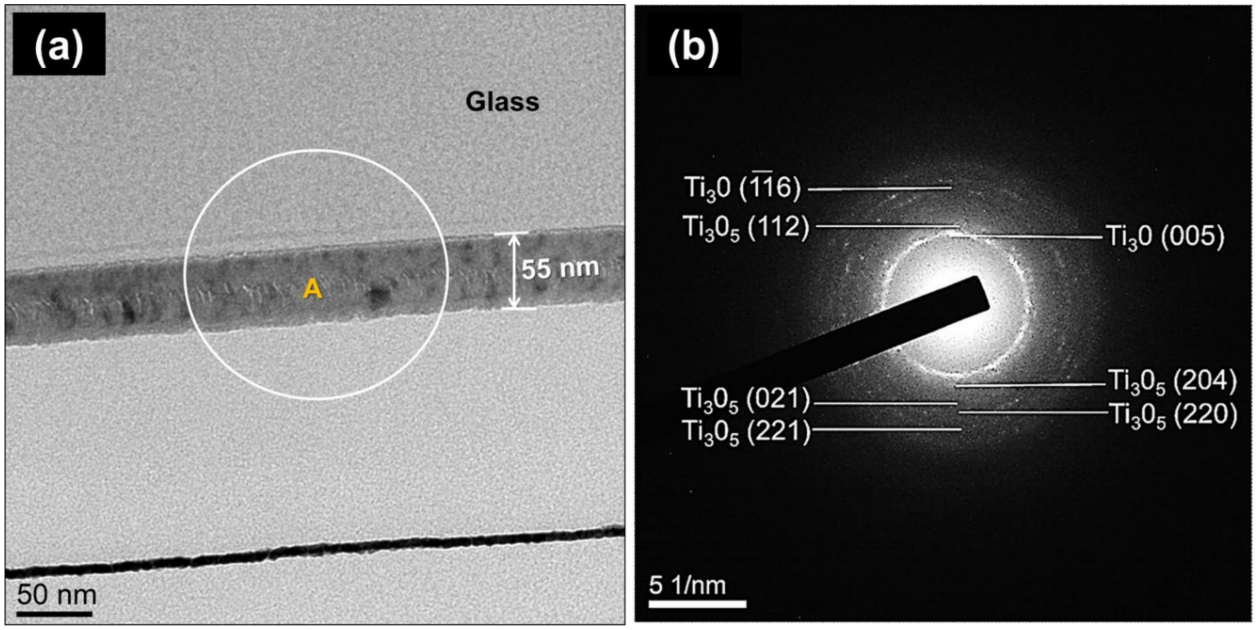

Figure 2. Cross-sectional HR-TEM images of Ti_3O_x thin-film sample deposit at 2 kW, (**a**) bright-field of the film with a thickness 55 nm. The image (inset A) was selected for electron diffraction analysis and (**b**) the selective area diffraction pattern of section "A" adjacent to Ti_3O and Ti_3O_5.

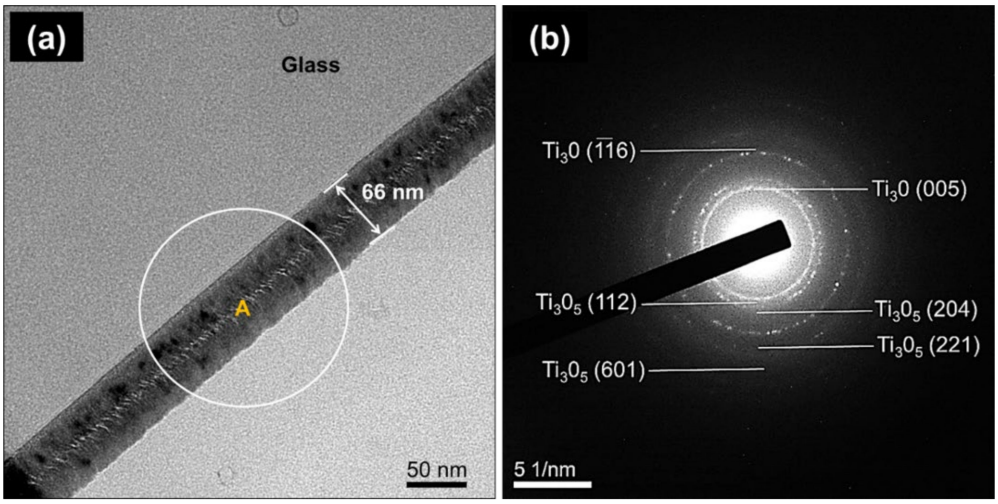

Figure 3. Cross-sectional HR-TEM images of Ti_3O_x thin-film sample deposit at 2.5 kW (**a**) bright-field of the film with a thickness 66 nm. The image (inset A) was selected for electron diffraction analysis, and (**b**) the selective area diffraction pattern of section "A" adjacent to Ti_3O and Ti_3O_5.

When Ti_3O_x films were annealed at 550 °C for 3 h, the Ti_3O/Ti_3O_5 phases were directly transferred to the rutile TiO_2 phase, as shown in Figure 4b. It shows that the films have good crystallinity. According to SAD pattern analysis, the crystalline planes (110), (211), and (101) belong to the rutile phase in the thin films. It has been reported that TiO_2 films can be prepared using sputtered titanium film by thermal oxidation [4,39,40]. The single-phase rutile TiO_2 can be obtained at 550 °C annealing, which agrees with the literature [28].

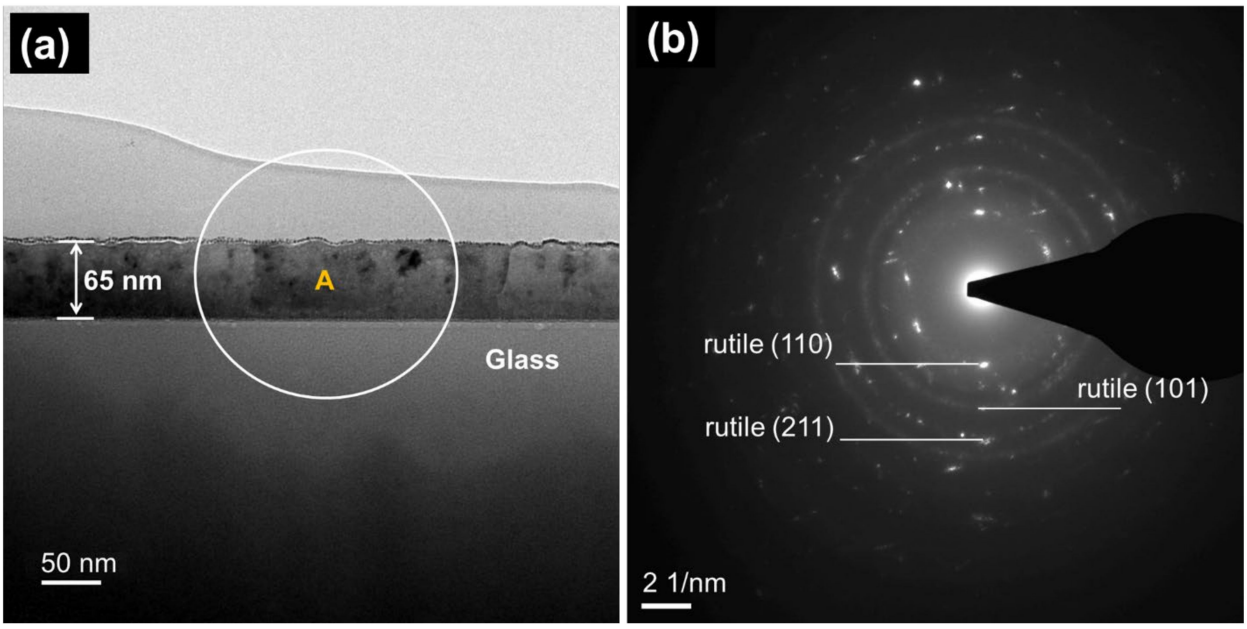

Figure 4. Cross-sectional HR-TEM images of TiO_2 thin-film (**a**) bright-field of the film with a thickness 65 nm. The image (inset A) was selected for electron diffraction analysis, and (**b**) the selective area diffraction pattern of section "A" adjacent to rutile TiO_2.

The influence of sputtering power on film chemical state, Ti2p, and O1s core level spectra of Ti_3O_x films were detected using X-ray photoelectron spectroscopy analysis (Figure 5). Photoelectron peaks for Ti and O were clearly recorded for all samples. XPS Ti^0 signals are 453.57 and 459.73 eV and Ti^{3+} signals are 457.1 and 463.1 eV, as shown on Figure 5a. The binding energy differences (ΔE_b) were found at 6.16 and 5.87 eV for Ti^0 and Ti^{3+}, respectively, which is in agreement with the literature [16,41]. After subtracting a Shirley background, the XPS spectra were fitted to the titanium oxide component and an asymmetric line-shape function to fit the metal component. Both Ti^0 (~453 eV) and Ti^{3+} (457.1 eV) chemical states in Ti_3O_x films have referred to Ti_3O and Ti_3O_5 phases. In addition, the binding energy curves observed at ~458 and ~463 eV correspond to Ti^{4+} that indicated TiO_2 phases. The shifted peak positions on TiO_2 films, shown in Figure 5a, indicate that the thermal annealing shifted the binding energy to higher values, effected by surface oxidation, and this effect ascribed to the O-Ti bonding [42].

Moreover, the increasing peak intensity of Ti^0 chemical state correlated with high metallic titanium when the sputtering power is increased from 2 to 2.5 kW. Godfroid et al. published that the films deposited at the high sputtering power attain the metallic state more rapidly [16].

Figure 5b shows an asymmetric high binding energy curve for O1s lines with an intense peak at 529 eV, which is in good agreement with a previous report [43]. The co-existence of Ti_3O and Ti_3O_5 phases in Ti_3O_x films was observed using HiPIMS at 2 kW and 2.5 kW with a low oxygen ratio (2.5%), indicating the Ti_3O_x films can be prepared at higher sputtering power and lower oxygen concentration. It is found that lower oxygen concentration plays a role in the co-existence of Ti_3O and Ti_3O_5 crystal phases. However, the O1s peak intensity was decreased significantly when the sputtering power increased from 2.0 kW to 2.5 kW.

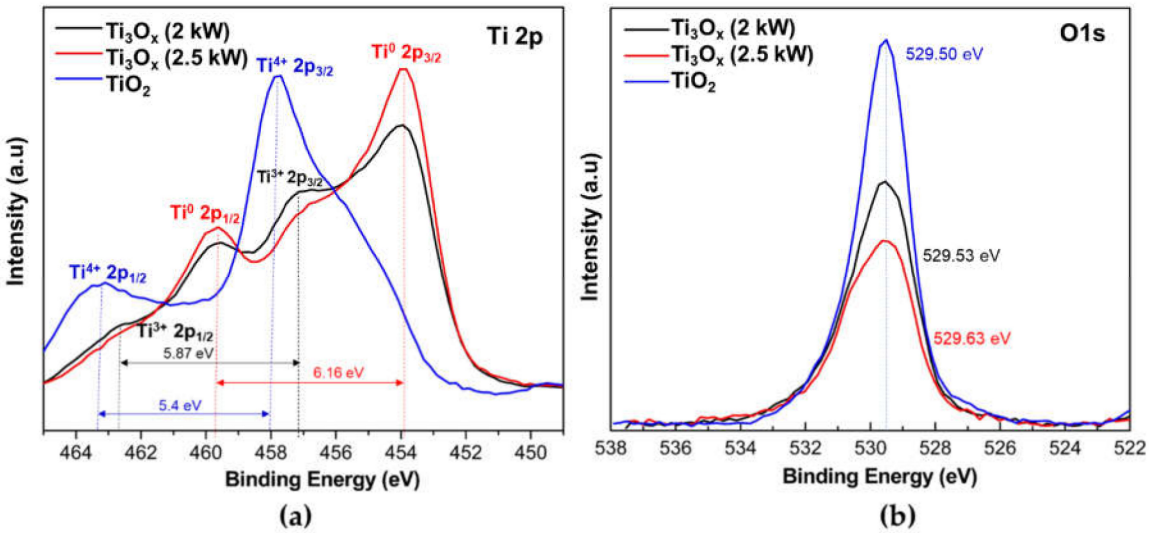

Figure 5. X-ray photoelectron spectroscopy of (**a**) Ti2p and (**b**) O1s spectra obtained from Ti_3O_x thin films deposit at 2 and 2.5 kW and TiO_2 thin films as a reference.

The chemical composition of Ti_3O_x films at different sputtering power was analyzed based on XPS data. The concentrations of titanium and oxygen are listed in Table 1. Ti to O proportion at different sputtering powers is 0.95 and 1.20 for 2 kV and 2.5 kV, respectively. The results indicate that the oxygen concentration in Ti_3O_x films was decreased with increasing sputtering power up to 2.5 kW. It means that the Ti_3O phase increased at 2.5 kV in the films. This result is consistent with the XRD and TEM analysis, as exhibited in Figures 1 and 3. Increasing the sputtering power up to 2.5 kW leads to shifting the binding energy to lower energy due to lower oxidation state changes in the Ti-O element. Furthermore, the atomic concentration of Ti and O in the TiO_2 films was 29.94 and 70.06%, respectively. Ti to O proportion is 0.42. More increased oxygen existence in TiO_2 films was expected after thermal annealing [44].

Table 1. Chemical composition of Ti_3O_x thin films.

Sample	Atomic Concentration (%)		Ti: O Ratio
	Ti	O	
Ti_3O_x (2 kW)	48.86	51.14	0.95
Ti_3O_x (2.5 kW)	54.67	45.33	1.20
TiO_2	29.94	70.06	0.42

2.2. Optical Properties and Photocatalytic Activity of Ti_3O_x Films

It is challenging to know the energy bandgap value for the Ti_3O_x films, while TiO_2 has an indirect bandgap with a value around 3.0–3.2 eV [24]. However, Ti_3O and Ti_3O_5 are still unknown. The indirect bandgap $\alpha\ hv = A\ (hv - E_g)^{0.5}$ was used to calculate the energy bandgap of Ti_3O_x films. The energy bandgap of TiO_2 films was used as a reference to compare with Ti_3O_x films. The energy bandgap of the Ti_3O_x films with different sputtering power is shown in Figure 6. The bandgap values of Ti_3O_x films are 3.36 and 3.50 eV for 2 and 2.5 kW, respectively. In this study, increasing the sputtering power up to 2.5 kW will lead to a monotonically increasing energy bandgap.

Indirect optical band gap in the range 3.58–3.75 eV with an increase in sputtering pressure in TiO_2 thin films being reported earlier by Prabitha et al. [45]. It is well known that the energy bandgap refers to the minimum energy needed to excite an electron from the bottom of the valence band to the top of the conduction band. The lower energy bandgap will lead to electrons excited into the conduction band from the valence band. However, it was found that the energy bandgap of Ti_3O_x films is higher than TiO_2 films

(3.10 eV). Generally, the energy bandgap (E*g*) of TiO_2 varies with its structure, with the E*g* of crystalline anatase and rutile phase being 3.2 and 3.0 eV, respectively [46].

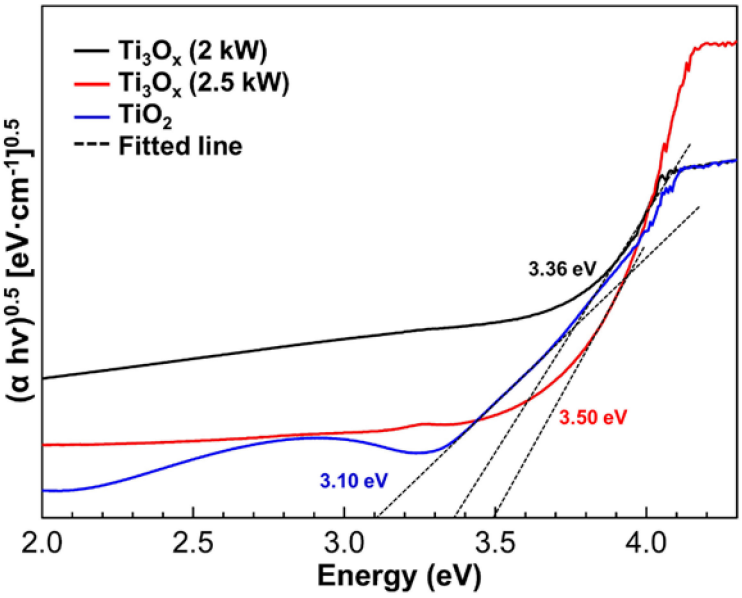

Figure 6. Indirect energy band gap value of the Ti_3O_x thin film deposited at 2 and 2.5 kW and TiO_2 thin film as reference.

The optical transmittance spectra of as-deposited Ti_3O_x films were measured using UV–Vis spectroscopy. Transmittance measurements as a function of wavelength are illustrated in Figure 7. Note that the TiO_2 films with 66 nm thickness were used as reference. The Ti_3O_x films exhibit low transmission in the spectral range 300–800 nm wavelength compared to TiO_2 films. The optical transmission spectra of the Ti_3O_x films showed feeble transmittance (<10%), while the sample with high sputtering power (2.5 kW) pointed almost no light transmission. TiO_2 films with equal thickness are highly transparent in the visible region, around 90%, and are relatively equal to glass substrate transmission spectra. According to microstructure analysis (Figures 2 and 3) of Ti_3O_x films, the intermixing of Ti_3O and Ti_3O_5 crystalline phases was observed in the films. These crystalline phases imply a lack of oxygen content in the films that causes poor light transmission. Moreover, the transmission of thin films correlates with the energy bandgap value. The bandgap of Ti_3O_x value is higher than TiO_2 thin films created the light was absorbed not transmitted [39]. It has been reported that the oxygen vacancies in TiO_2 film enhanced the absorption of visible light [25].

The photocatalytic activities of Ti_3O_x films deposited at 2 and 2.5 kW were investigated by degradation of methylene blue solution as shown in Figure 8. When the samples were irradiated by UV light, the absorbance of MB decreased, which indicates that the films performed photocatalytic properties. TiO_2 films with similar thickness and preparation were used to compare the photocatalytic activity. It can be observed that all the samples exhibited quick absorption in the dark. This could be attributed to the high specific surface and small particle size [47] as shown in Figure 8a, The methylene blue degradation of the substrate as control was ~18% (Figure 8a). After UV irradiation, the samples show has a good degradation performance with a range of 51–61% compared to the substrate.

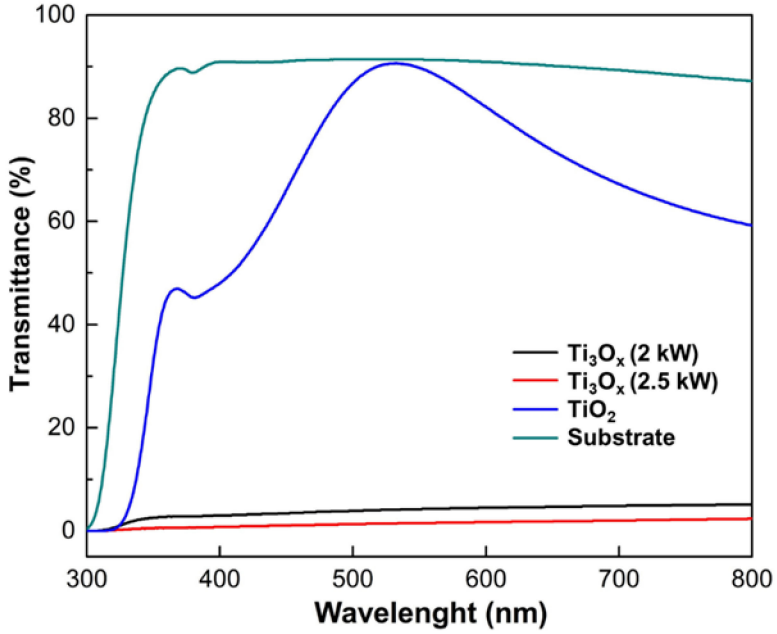

Figure 7. UV–Vis transmittance spectra of the Ti_3O_x thin film deposited at 2 and 2.5 kW compared with TiO_2 thin film.

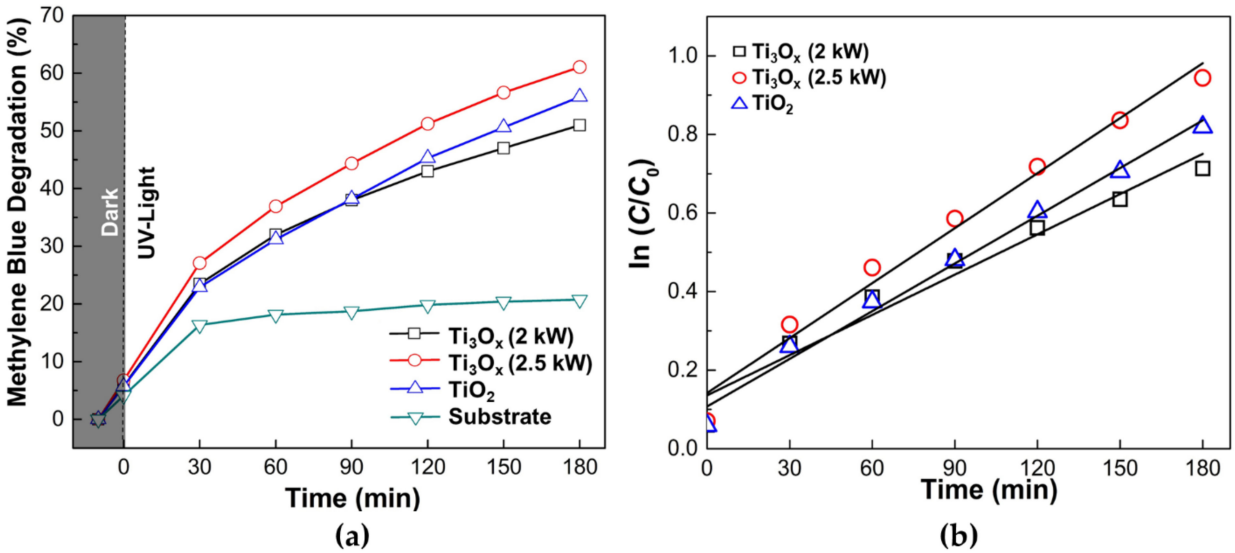

Figure 8. Photocatalytic activity of Ti_3O_x thin film samples in the function of the irradiation time in MB solution. (**a**) Methylene blue degradation percentage. (**b**) First-order reaction rate of thin films samples with MB.

The degradation percentage of methylene blue solution with Ti_3O_x thin films with 2.5 kW sputtering power has higher photocatalytic activity than 2 kW. According to the HR-TEM and XRD analysis, Ti_3O and Ti_3O_5 crystalline phases co-existed in the films, and the crystalline phases increased with increasing sputter power, as displayed in Figure 3. Interestingly, the Ti_3O_x films with 2.5 kW sputtering power have a higher photocatalytic activity (61.0%) compared with TiO_2 films (55.9%) at a similar thickness. This indicates that the Ti_3O_x phases exhibit higher photocatalytic activity than TiO_2 (rutile) films at similar thickness. Qi et al. [36] reported that UV light could stimulate the Ti_3O_5 to produce electron–hole pairs and help redox reactions. The photogenerated electrons will interact with molecular oxygen (O_2) to generate superoxide radical anions (O_{2-}), and the photogenerated holes react with water to form hydroxyl (·OH) radicals. Ti_3O_x films prepared

by this HiPIMS technique at 2.5 kW and low oxygen ratio (2.5%) demonstrated good photocatalytic activity.

According to first-order reaction kinetics (as shown in Figure 8b), the time-dependent $\ln(C/C_0)$ terms are illustrated for all the film samples. The reaction rate constants (k) of the Ti_3O_x films and TiO_2 were calculated: Ti_3O_x films at 2 kW, 2.5 kW, TiO_2 film were 3.42×10^{-3} min^{-1},4.67×10^{-3} min^{-1}, and 4.05×10^{-3} min^{-1}, respectively. These results explain that a higher degradation rate can be obtained for Ti_3O_x films sputtered at 2.5 kW. The reaction constants (k) gradually increased with an increasing the Ti_3O_x film thickness. Influencing significant effects on the electronic, photonic, and photocatalytic properties of TiO_2, oxygen deficiencies are critical features [48–50].

The schematic diagram of photocatalytic reaction for MB removal by Ti_3O_x thin films is illustrated in Figure 9. The valence bandgap (*vb*) and conduction band (*cb*) of Ti_3O_x thin films around 3.5 eV. When Ti_3O_x is exposed to energy light (*hv*) that is larger than the thin film's energy bandgap, the electron (e^-) in the *vb* will migrate to the *cb*, retaining a positive hole (h^+) in the *vb*. These exciting holes and electrons have high energy potentials that can transfer to the semiconductor's surface, producing strong reactive free radicals or recombining. Water (H_2O) and oxygen (O_2) molecules will be trapped on the semiconductor surface by an exciting hole in *vb* and an excited electron in *cb*, respectively. Finally, trapped H_2O is oxidized into highly reactive hydroxyl radicals (OH•) at *vb*, whereas oxygen is reduced into superoxide radical ion ($O_2^{\bullet-}$) at *cb*. These processes may accelerate the photocatalytic process and MB degradation [51].

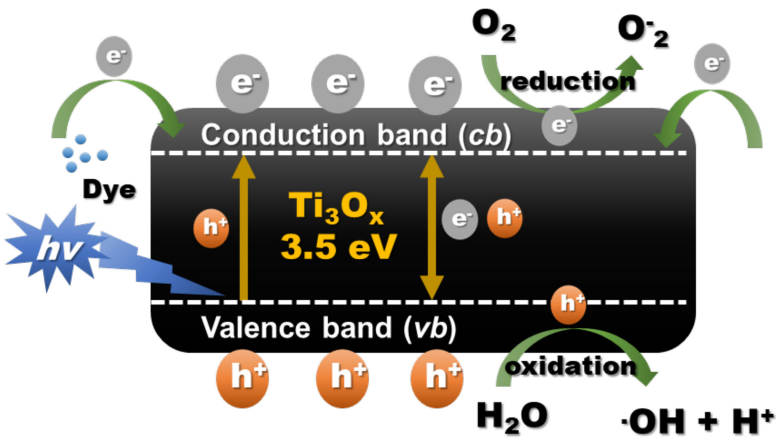

Figure 9. Schematic diagram energy bandgap of Ti_3O_x thin films showing the charge transportation process leading to light irradiation-driven photocatalytic degradation of methylene blue.

Film thickness and energy bandgap are two key factors determining the photocatalytic performance of Ti_3O_x thin films. The energy bandgap of Ti_3O_x thin films is ~3.5 eV, which is higher than the rutile (3.0 eV) or anatase (3.2 eV) phases. According to Qutub et al. [52], the photocatalytic activity of semiconductor particles in aqueous solutions is conducted by electrons and holes produced by photo-excitation. As electrons prefer to recombine with positive holes, the photogenerated electrons should be efficiently separated from the holes to enhance photocatalytic efficiency. One of the effective approaches is to increase the semiconductor catalyst's bandgap, which minimizes the recombination of electrons and holes. In addition, a higher bandgap also corresponds to promoting high redox ability [53]. As the Ti_3O_x has a higher bandgap than rutile TiO_2, its oxidizing ability should be stronger. Therefore, Ti_3O_x has a higher energy bandgap promoting better photocatalytic performance than rutile TiO_2 thin films. However, the Ti_3O_x deposited at 2 kW showed lower photocatalytic activity than TiO_2 even though it has a higher energy bandgap (3.36 eV). A possible reason is that the film thickness of Ti_3O_x deposited at 2 kW is lower than TiO_2 thin films.

These outcomes indicated that increasing the deposition power up to 2.5 kW can promote high thickness of Ti_3O_x thin films with energy band gap of ~3.5 eV thus showing

high photocatalytic performance. Furthermore, semiconducting photocatalysts mainly depend upon separating a photogenerated hole–electron pairs and transferring electrons from the photocatalyst into the organic pollutants within the oxygen vacancy defects on the surface [54,55].

2.3. Antibacterial Activity of Ti_3O_x Films

The results of the antibacterial activity of *E. coli* (Gram-negative) and *S. aureus* (Gram-positive) on Ti_3O_x thin films compared to glass substrate and antibiotic are presented in Figure 10. The initial concentration of bacteria was 1×10^5 CFU/mL. The glass substrate under UV light only showed a minor antibacterial activity on *E. coli* and *S. aureus* (less than 16%). Instead, the group treated with an antibiotic (100 μg/mL) as positive control showed high antibacterial inhibition for both bacteria. Notably, two kinds of Ti_3O_x thin-film presented significant antibacterial effects against *E. coli* and *S. aureus* ($p < 0.05$) with bactericidal rates around 80 and 90% in the presence of UV light, respectively (Figure 9).

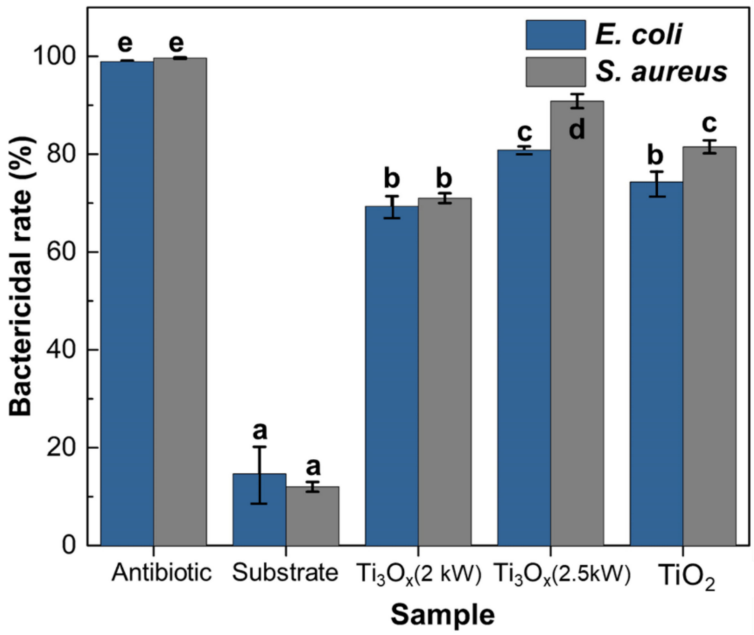

Figure 10. Effect of Ti_3O_x thin films on bactericidal activity against *E. coli* and *S. aureus* compared to the substrate (negative control) and antibiotic (100 μg/mL, positive control) after 60 min UV light irradiation treatment. Means denoted by a different letter indicate significant differences between treatments ($p < 0.05$; Tukey HSD test). Data were expressed as mean ± standard deviation ($n = 3$).

It could be seen that the bactericidal rate for both *E. coli* and *S. aureus* significantly increases remarkably with sputtering power increases up to 2.5 kW after 60 min of UV irradiation. The antibacterial effect of Ti_3O_x thin films on *E. coli* and *S. aureus* can be ascribed both to the UV irradiation and photocatalytic activity of Ti_3O_x thin films containing crystal structures of Ti_3O_5 and Ti_3O. The thin films fabricated with higher sputtering power (2.5 kW) showed a higher bactericidal rate. The increasing thickness of Ti_3O_x thin films is effective for the inactivation of both Gram-positive and Gram-negative bacteria, and the antibacterial ability of the films Ti_3O_x (2.5 kW) is even better than the rutile TiO_2 film (74%). The results indicate that the antimicrobial activity depended on the UV irradiation and sputtering power of Ti_3O_x thin films.

Numerous studies have reported the antibacterial activity of TiO_2 thin films. However, there has been limited published work that refers to the antibacterial mechanism on Ti_3O_x thin films. According to Sunada et al. [56], the bactericidal process comprises low-rate photo-killing and high-rate photo-killing stages. The low-rate photo-killing stage is the partial destruction of the outer membrane of bacteria through robust reactive oxygen species (ROS) produced by TiO_2. Several investigations have shown that ROS

formation is the primary mechanism responsible for the antibacterial activities of TiO_2-based materials [56–59]. Generation of reactive oxygen species (ROS) occurs due to the induction of electron–hole pairs under light radiation, which recombine and release energy as heat or dissociate due to the charge trapping, thus creating charge carriers for redox reactions in the photocatalytic process.

Photoexcited electron–hole pairs interact with adsorbed electron donors and acceptors (water and oxygen) on the TiO_2 surface to generate highly reactive hydroxyl radicals (OH•) and superoxide ions ($O_2^{\bullet -}$) during the photocatalytic process as described in Figure 9. These two reactive oxygen species are strong oxidants that can degrade and oxidize organic material, including bacteria. This process has significant effect on cell mortality. Furthermore, it alters cell permeability, allowing ROS to be more easily accessible to the cell membrane. As a result, ROS attach to the cell membrane, accelerating the peroxidation of the cell membrane's polyunsaturated phospholipid layer. This process will result in the loss of respiratory activity and the leaking of cell components, which will eventually lead to cell death [60,61]. In addition, the formation of such Magnéli phase in a previous study could contribute to the enhanced antibacterial properties observed under irradiation light [31].

Moreover, the bactericidal activity on Ti_3O_x thin films is statistically significantly higher on *S. aureus* (90.83%) than *E. coli* (80.83%), as presented in Figure 10. According to Russell [62], Gram-negative bacteria such as *E. coli* are less sensitive to ROS than Gram-positive bacteria (*S. aureus*). The structural differences in the bacterial cell membrane are one of the primary causes of the increased resistance. Cell membranes of Gram-positive bacteria are covered by a membrane predominantly composed of a peptidoglycan layer and teichoic and lipoteichoic acids. Gram-positive bacteria have a membrane surrounding the cell wall that is composed primarily of a thick peptidoglycan layer and teichoic and lipoteichoic acids but no outer lipid membrane. However, the cell membrane of Gram-negative bacteria is more complex due to an outer membrane composed mainly of lipopolysaccharide (LPS) and a thin peptidoglycan layer [63]. The outer membrane serves as the first barrier, and once it is breached, the cytoplasmic membrane is targeted, resulting in a reduction in cellular respiration and, finally, the death of cells. Consequently, the outer membrane of Gram-negative bacteria works as a permeability barrier, reducing the absorption of reactive oxygen species (ROS) into the cell [62].

These results indicated that deposition power plays crucial parameters for obtaining high photocatalytic performance and antibacterial activity of Ti_3O_x films from our studies. Furthermore, sputtering power at 2.5 kW could provide a high thickness of Ti_3O_x films with an energy bandgap of ~3.4 eV and exhibited higher photocatalytic activity than TiO_2 thin films. Thus, the study demonstrated that the intermixing of the Ti_3O and Ti_3O_5 phase on thin-film could promote a high photocatalytic and antibacterial activity that could be considered as an efficient and lasting antibacterial material for future antibacterial and biomedical application.

3. Materials and Methods

3.1. Preparation of Ti_3O_x Thin Films

The Ti_3O_x thin films were deposited onto the glass substrate using reactive HiPIMS. Glass substrate size was 76 × 25 mm and ultrasonically cleaned in acetone, ethanol, and deionized water for 30 min in sequence before the deposition process. Then, it was blown dry with air and put on holders. Titanium layers were deposited at sputtering power 2 and 2.5 kW using a 99.99% purity titanium target (Ultimate materials Technology Co., Ltd., Hsinchu, Taiwan) with dimensions 550 × 125 mm and thickness 6 mm. The target to substrate distance was kept constant at 150 mm. High-purity oxygen (99.99%) and argon (99.99%) were used as reactive and working gas, respectively. Reactive sputter deposition was operated at 2.7×10^{-3} Torr (0.36 pa) working pressure, the substrate temperature was controlled at 25 °C, and the flow rate of argon and oxygen was fixed at 200 and 5 sccm, respectively. All Ti_3O_x thin film samples were prepared without a post-annealing process.

Moreover, the TiO_2 thin films sample was developed as a comparable sample for Ti_3O_x thin films. TiO_2 thin films with thickness around 65 nm were prepared from Ti_3O_x thin films (2.5 kW; 5 sccm) samples that continue with post-annealing at 550 °C for 3 h. A summary of the parameters and deposition conditions of Ti_3O_x thin film is given in Table 2.

Table 2. The deposition rate and thickness of Ti_3O_x thin film deposited at 2- and 2.5 kW.

Sputtering Power (kW)	Argon Flow (sccm)	Oxygen Flow (sccm)	Deposition Rate (nm/min)	Thickness (nm)
2	200	5	99	55
2.5	200	5	119	66

3.2. Sample Characterization

The crystal phase was determined using X-ray diffraction (XRD; Bruker D8 Advance-AXS Gmbh, Am Studio 2D, Berlin, Germany) with monochromatic Cu-Kα radiation (λ = 1.541 Å), operated at 40 kV and 40 mA. The 2θ scan range is between $10° \leq 2\theta \leq 60°$ with a grazing angle of 0.1° and a scan speed of 5 s. Microstructural and film thickness observation of the cross-sectional and plane-view morphology of the films deposited onto a glass substrate was observed using a Field Emission Gun Transmission Electron Microscopy (FEG-TEM; FEI E.O Tecnai F20, FEI Company—Thermo Fisher Scientific, Hillsboro, OR, USA) equipped with charge-coupled device (CCD) camera. Selected area diffraction (SAD) was employed at an acceleration voltage of 200 kV. The evaluation of high-resolution TEM (HR-TEM) and SAD patterns was conducted using the Gatan Digital Micrograph software package (version 2.11.1404.0) (Gatan Inc., Pleasanton, CA, USA). The interplanar distance in the real spaces (d-spacing) that were observed from software was compared with the crystallographic database of the Ti_3O and Ti_3O_5 planes from JCPDS. The films' quantitative composition on the surface and internal area was examined with X-ray photoelectron spectroscopy (XPS; JEOL, JPS-9010MX, JEOL Ltd, Tokyo, Japan). Internal profile experiments were performed by sputter etching rate 28 nm/min in the thin film for 20 s. Then, the analyzer was operated at voltage 10 kV and current 5 mA with Mg Kα radiation line. The X-ray photoelectron spectra were referenced to the C 1s peak (E_b = 285 eV) present on the sample surface.

3.3. Optical Properties Characterization

The absorbance and transmittance of Ti_3O_x thin films were determined using UV-vis spectrophotometer (UV/Vis, U-3310, Hitachi Ltd., Tokyo, Japan) in the range wavelength 200–1000 nm and 300–800 nm, respectively. The energy bandgap of the thin films was estimated from the Tauc plots of the optical absorbance. The determination of the energy bandgap was obtained by Tauc's Equation [64,65] Equation (1):

$$\alpha\, hv = A\,\left(hv - E_g\right)^n \tag{1}$$

where α is the absorbed coefficient, h is the Planck constant, ν is the photon's frequency, A is a constant proportionality, E_g is the allowed energy gap, and n = 0.5 for allowed direct transition.

The photocatalytic activity of thin films was evaluated by measuring the degradation of Methylene Blue (MB Alfa Aesar; Thermo Fisher Scientific, Lancashire, UK) in the presence of UV light. Ti_3O_x Thin-film samples with size 26 mm × 38 mm were immersed into 20 mL aqueous MB solution with an initial concentration (C) of 10 mg/L then irradiated using UV lamp 8 W (UV T8; Philip, Amsterdam, The Netherlands) for 3 h. The UV source was 9 cm from the thin films. Prior to UV radiation, the film was immersed in MB solution and kept under dark conditions for 10 min to achieve MB absorption equilibrium on the Ti_3O_x and TiO_2 layer. From the end of the dark-storage time (t = 0 min, C_0), a sample of dye solution was analyzed every 30 min for 3 h (t = 30–180 min, C_{30} to C_{180}). The Ti_3O_x film photocatalytic activity was determined using UV–Vis spectrophotometer (UV/Vis,

U-3310, Hitachi Ltd., Tokyo, Japan) based on the change in MB concentration following the UV irradiation time (the maximum absorption wavelength of the dye at 664 nm), as described in a previous report [4,28,66]. The degradation of methylene blue was estimated by calculating the percentage of the dye concentration that remained over (C_0) the initial dye concentration (C), obtained from the absorbance standard curve. The degradation performance evaluated by considering the following Equation (2):

$$\textit{Methylene Blue Degradation } (\%) = \left[1 - \left(\frac{C_0}{C}\right)\right] \times 100 \quad (2)$$

The initial and final concentrations of methylene blue (mg/L) at reaction time (t) were C and C_0, respectively. In the pseudo-first-order photodegradation kinetics, the $\ln(C/C_0)$ linear fit slope in the function of time plot represents the kinetic constant (k) of the photodegradation, which can be found in Equation (3):

$$\ln \frac{C}{C_0} = -kt \quad (3)$$

3.4. Antibacterial Activity

The antibacterial activity of the Ti_3O_x thin films was evaluated by the agar dilution method [67] against Gram-negative *Escherichia coli* (ATCC25922) and Gram-positive bacteria *Staphylococcus aureus* (ATCC10234). The bacteria were grown in Tryptic Soy Broth (DIFCO^{tm}, Becton Dickirnson and Company sparks, Maryland, USA) at 37 °C for 12 h. The initial cell concentration used for antibacterial activity was about 1×10^5 colony-forming units (CFU)/mL. Thin films samples with dimensions 1 × 1 cm were placed in sterilized 12 welled plates (SPL Life Sciences Co., Ltd., Gyeonggi-do, Korea). Furthermore, 40 µL of the bacterial solution was dropped on the surface of the thin films. The plates were sealed then UV-irradiated (UV-A, 8 W T8; λ = 365 nm, Philip, Amsterdam, The Netherlands) for 60 min at room temperature (25 ± 2 °C). After finishing, 10 µL of the remaining sample on the thin-film was taken, and serial dilution was performed. The aliquots of serially diluted suspensions were plated on Tryptic Soy Agar (DIFCO^{tm}, Becton Dickirnson and Company sparks, MD, USA) plates and incubated at 37 °C for 24 h, and the number of colonies on the plates was counted. In order to compare antibacterial activity, substrate (glass) and antibiotic (100 µg/mL, kanamycin and ampicillin, Sigma-Aldrich, MO, USA)) were used as a negative and positive control. The same treatment was done under dark conditions. The experiment was done in triplicate. All of the experiment was conducted in a sterile environment. The bactericidal rate (K) was calculated by Equation (4):

$$K = \left(\frac{A - B}{A}\right) \times 100 \quad (4)$$

A and B are the numbers of original bacteria colonies grown in the culture medium corresponding to the sample after irradiation with UV light, respectively.

One-way analysis of variance (ANOVA) was performed by using 'SPSS Statistics' version 16 software (SPSS for Windows; IBM Corp, New York, NY, USA). Post hoc testing was done using Tukey HSD tests, which were done to determine significant group differences in antibacterial analysis, and means were considered statistically significant if $p < 0.05$. Data were expressed as mean ± standard deviation.

4. Conclusions

The Ti_3O_x films can be prepared using the reactive High-Power Impulse Magnetron Sputtering (HiPIMS) method without post-thermal annealing. There are two phases (Ti_3O and Ti_3O_5) that co-existed in the Ti_3O_x films. The sputtering power played a role in influencing the structure, morphology, optical, and photocatalytic properties of Ti_3O_x thin films. It was found that increasing the sputtering power up to 2.5 kW leads to increased crystalline intensity of Ti_3O and Ti_3O_5. The Ti_3O_x films with 2.5 kW sputtering power could

promote higher photocatalytic and antibacterial activity against Gram-negative and Gram-positive bacteria compared with TiO_2 films. Therefore, the Ti_3O_x thin film photocatalyst is an attractive and long-lasting antibacterial material appropriate to future biomedical and bactericidal applications.

Author Contributions: Conceptualization, Y.-C.L. and J.-L.H.; methodology, F.-Y.X.; software, J.-H.J.; validation, C.-T.C.; formal analysis, E.W. and F.-Y.X.; investigation, E.W.; resources, Y.-C.L. and J.-L.H.; data curation, C.-T.C.; writing—original draft preparation, E.W.; writing—review and editing, E.W. and Y.-C.L.; visualization, E.W. and J.-H.J.; supervision, Y.-C.L. and J.-L.H.; funding acquisition, Y.-C.L. All authors have read and agreed to the published version of the manuscript.

Funding: This research received no external funding.

Data Availability Statement: Data are contained within the article.

Acknowledgments: The author wishes to thank the TaiwanICDF for Ph.D. scholarship funding; Douglas J.H. Shyu and Liyu Chiang from Dept. Biological Science and technology, NPUST, Taiwan, for providing a bacterial culture; and the National Sun Yat-sen University staff for assistance with XPS (Instrument ID: ESCA00002100) experiments. This research did not receive any specific grant from funding agencies in agencies in the public, commercial, or non-profit sectors.

Conflicts of Interest: The authors declare no conflict of interest.

References

1. Huang, C.Y.; Selvaraj, P.; Senguttuvan, G.; Hsu, C.J. Electro-optical and dielectric properties of TiO_2 nanoparticles in nematic liquid crystals with high dielectric anisotropy. *J. Mol. Liq.* **2019**, *286*, 110902. [CrossRef]
2. Banerjee, S.; Dionysiou, D.D.; Pillai, S.C. Self-cleaning applications of TiO_2 by photo-induced hydrophilicity and photocatalysis. *Appl. Catal. B Environ.* **2015**, *176*, 396–428. [CrossRef]
3. Kathirvel, S.; Pedaballi, S.; Su, C.; Chen, B.-R.; Li, W.-R. Morphological control of TiO_2 nanocrystals by solvothermal synthesis for dye-sensitized solar cell applications. *Appl. Surf. Sci.* **2020**, *519*, 146082. [CrossRef]
4. Lee, P.-Y.; Widyastuti, E.; Lin, T.-C.; Chiu, C.-T.; Xu, F.-Y.; Tseng, Y.-T.; Lee, Y.-C. The phase evolution and photocatalytic properties of a Ti-TiO_2 bilayer thin film prepared using thermal oxidation. *Coatings* **2021**, *11*, 808. [CrossRef]
5. Lu, Y.; Matsuda, Y.; Sagara, K.; Hao, L.; Otomitsu, T.; Yoshida, H. Fabrication and Thermoelectric Properties of Magneli Phases by Adding Ti into TiO_2. In *Proceedings of the Advanced Materials Research*; Trans Tech Publications Ltd: Zurich, Switzerland, 2012; Volume 415, pp. 1291–1296.
6. Huang, S.-S.; Lin, Y.-H.; Chuang, W.; Shao, P.-S.; Chuang, C.-H.; Lee, J.-F.; Lu, M.-L.; Weng, Y.-T.; Wu, N.-L. Synthesis of high-performance titanium sub-oxides for electrochemical applications using combination of sol–gel and vacuum-carbothermic processes. *ACS Sustain. Chem. Eng.* **2018**, *6*, 3162–3168. [CrossRef]
7. Xu, B.; Sohn, H.Y.; Mohassab, Y.; Lan, Y. Structures, preparation and applications of titanium suboxides. *RSC Adv.* **2016**, *6*, 79706–79722. [CrossRef]
8. Pabón, B.M.; Beltrán, J.I.; Sánchez-Santolino, G.; Palacio, I.; López-Sánchez, J.; Rubio-Zuazo, J.; Rojo, J.M.; Ferrer, P.; Mascaraque, A.; Muñoz, M.C. Formation of titanium monoxide (001) single-crystalline thin film induced by ion bombardment of titanium dioxide (110). *Nat. Commun.* **2015**, *6*, 1–6. [CrossRef]
9. Fusi, M.; Maccallini, E.; Caruso, T.; Casari, C.S.; Bassi, A.L.; Bottani, C.E.; Rudolf, P.; Prince, K.C.; Agostino, R.G. Surface electronic and structural properties of nanostructured titanium oxide grown by pulsed laser deposition. *Surf. Sci.* **2011**, *605*, 333–340. [CrossRef]
10. Lackner, J.M.; Waldhauser, W.; Ebner, R.; Major, B.; Schöberl, T. Pulsed laser deposition of titanium oxide coatings at room temperature—Structural, mechanical and tribological properties. *Surf. Coatings Technol.* **2004**, *180*, 585–590. [CrossRef]
11. Farstad, M.H.; Ragazzon, D.; Grönbeck, H.; Strømsheim, M.D.; Stavrakas, C.; Gustafson, J.; Sandell, A.; Borg, A. TiO_x thin films grown on Pd (100) and Pd (111) by chemical vapor deposition. *Surf. Sci.* **2016**, *649*, 80–89. [CrossRef]
12. Greczynski, G.; Petrov, I.; Greene, J.E.; Hultman, L. Paradigm shift in thin-film growth by magnetron sputtering: From gas-ion to metal-ion irradiation of the growing film. *J. Vac. Sci. Technol. A* **2019**, *37*, 60801. [CrossRef]
13. Horprathum, M.; Eiamchai, P.; Chindaudom, P.; Pokaipisit, A.; Limsuwan, P. Oxygen partial pressure dependence of the properties of TiO_2 thin films deposited by DC reactive magnetron sputtering. *Procedia Eng.* **2012**, *32*, 676–682. [CrossRef]
14. Okimura, K. Low temperature growth of rutile TiO_2 films in modified rf magnetron sputtering. *Surf. Coatings Technol.* **2001**, *135*, 286–290. [CrossRef]
15. Gouttebaron, R.; Cornelissen, D.; Snyders, R.; Dauchot, J.P.; Wautelet, M.; Hecq, M. XPS study of TiO_x thin films prepared by dc magnetron sputtering in Ar–O_2 gas mixtures. *Surf. Interface Anal.* **2000**, *30*, 527–530. [CrossRef]
16. Godfroid, T.; Gouttebaron, R.; Dauchot, J.P.; Leclere, P.; Lazzaroni, R.; Hecq, M. Growth of ultrathin Ti films deposited on SnO_2 by magnetron sputtering. *Thin Solid Films* **2003**, *437*, 57–62. [CrossRef]

17. Tiron, V.; Velicu, I.-L.; Dobromir, M.; Demeter, A.; Samoila, F.; Ursu, C.; Sirghi, L. Reactive multi-pulse HiPIMS deposition of oxygen-deficient TiO_x thin films. *Thin Solid Films* **2016**, *603*, 255–261. [CrossRef]
18. Greczynski, G.; Mráz, S.; Hans, M.; Primetzhofer, D.; Lu, J.; Hultman, L.; Schneider, J.M. Unprecedented Al supersaturation in single-phase rock salt structure VAlN films by Al^+ subplantation. *J. Appl. Phys.* **2017**, *121*, 171907. [CrossRef]
19. Zauner, L.; Ertelthaler, P.; Wojcik, T.; Bolvardi, H.; Kolozsvári, S.; Mayrhofer, P.H.; Riedl, H. Reactive HiPIMS deposition of Ti-Al-N: Influence of the deposition parameters on the cubic to hexagonal phase transition. *Surf. Coatings Technol.* **2020**, *382*, 125007. [CrossRef]
20. Mareš, P.; Dubau, M.; Polášek, J.; Mates, T.; Kozák, T.; Vyskočil, J. High deposition rate films prepared by reactive HiPIMS. *Vacuum* **2021**, *191*, 110329. [CrossRef]
21. Depla, D.; Heirwegh, S.; Mahieu, S.; De Gryse, R. Towards a more complete model for reactive magnetron sputtering. *J. Phys. D Appl. Phys.* **2007**, *40*, 1957. [CrossRef]
22. Lou, B.-S.; Yang, Y.-C.; Qiu, Y.-X.; Diyatmika, W.; Lee, J.-W. Hybrid high power impulse and radio frequency magnetron sputtering system for TiCrSiN thin film depositions: Plasma characteristics and film properties. *Surf. Coatings Technol.* **2018**, *350*, 762–772. [CrossRef]
23. Pansila, P.; Witit-Anun, N.; Chaiyakun, S. Influence of sputtering power on structure and photocatalyst properties of DC magnetron sputtered TiO_2 thin film. *Procedia Eng.* **2012**, *32*, 862–867. [CrossRef]
24. Kamble, S.S.; Radhakrishnan, J.K. Influence of O_2 flow rate on the characteristics of TiO_2 thin films deposited by RF reactive sputtering. *Mater. Today Proc.* **2020**, *33*, 709–715. [CrossRef]
25. Sério, S.; Jorge, M.E.M.; Maneira, M.J.P.; Nunes, Y. Influence of O_2 partial pressure on the growth of nanostructured anatase phase TiO_2 thin films prepared by DC reactive magnetron sputtering. *Mater. Chem. Phys.* **2011**, *126*, 73–81. [CrossRef]
26. Fan, Y.; Zhang, C.; Liu, X.; Lin, Y.; Gao, G.; Ma, C.; Yin, Y.; Li, X. Structure and transport properties of titanium oxide (Ti_2O, $TiO_{1+\delta}$, and Ti_3O_5) thin films. *J. Alloys Compd.* **2019**, *786*, 607–613. [CrossRef]
27. Ohkoshi, S.; Tsunobuchi, Y.; Matsuda, T.; Hashimoto, K.; Namai, A.; Hakoe, F.; Tokoro, H. Synthesis of a metal oxide with a room-temperature photoreversible phase transition. *Nat. Chem.* **2010**, *2*, 539. [CrossRef]
28. Shang, J.T.; Chen, C.M.; Cheng, T.C.; Lee, Y.C. Influences of annealing temperature on microstructure and properties for TiO_2 films deposited by DC magnetron sputtering. *Jpn. J. Appl. Phys.* **2015**, *54*, 125501. [CrossRef]
29. Starbova, K.; Yordanova, V.; Nihtianova, D.; Hintz, W.; Tomas, J.; Starbov, N. Excimer laser processing as a tool for photocatalytic design of sol–gel TiO_2 thin films. *Appl. Surf. Sci.* **2008**, *254*, 4044–4051. [CrossRef]
30. Domaschke, M.; Zhou, X.; Wergen, L.; Romeis, S.; Miehlich, M.E.; Meyer, K.; Peukert, W.; Schmuki, P. Magnéli-phases in anatase strongly promote cocatalyst-free photocatalytic hydrogen evolution. *ACS Catal.* **2019**, *9*, 3627–3632. [CrossRef]
31. Morakul, S.; Otsuka, Y.; Ohnuma, K.; Tagaya, M.; Motozuka, S.; Miyashita, Y.; Mutoh, Y. Enhancement effect on antibacterial property of gray titania coating by plasma-sprayed hydroxyapatite-amino acid complexes during irradiation with visible light. *Heliyon* **2019**, *5*, e02207. [CrossRef]
32. Abir, M.M.M.; Otsuka, Y.; Ohnuma, K.; Miyashita, Y. Effects of composition of hydroxyapatite/gray titania coating fabricated by suspension plasma spraying on mechanical and antibacterial properties. *J. Mech. Behav. Biomed. Mater.* **2021**, *125*, 104888. [CrossRef] [PubMed]
33. Matsuya, T.; Morakul, S.; Otsuka, Y.; Ohnuma, K.; Tagaya, M.; Motozuka, S.; Miyashita, Y.; Mutoh, Y. Visible light-induced antibacterial effects of the luminescent complex of hydroxyapatite and 8-hydroxyquinoline with gray titania coating. *Appl. Surf. Sci.* **2018**, *448*, 529–538. [CrossRef]
34. Ould-Hamouda, A.; Tokoro, H.; Ohkoshi, S.-I.; Freysz, E. Single-shot time resolved study of the photo-reversible phase transition induced in flakes of Ti_3O_5 nanoparticles at room temperature. *Chem. Phys. Lett.* **2014**, *608*, 106–112. [CrossRef]
35. Liu, R.; Shang, J.-X.; Wang, F.-H. Electronic, magnetic and optical properties of β-Ti_3O_5 and λ-Ti_3O_5: A density functional study. *Comput. Mater. Sci.* **2014**, *81*, 158–162. [CrossRef]
36. Qi, W.; Du, J.; Peng, Y.; Wang, Y.; Xu, Y.; Li, X.; Zhang, K.; Gong, C.; Luo, M.; Peng, H. Self-induced preparation of Ti_3O_5 nanorods by chemical vapor deposition. *Vacuum* **2017**, *143*, 380–385. [CrossRef]
37. Sun, P.; Hu, X.; Wei, G.; Wang, R.; Wang, Q.; Wang, H.; Wang, X. Ti_3O_5 nanofilm on carbon nanotubes by pulse laser deposition: Enhanced electrochemical performance. *Appl. Surf. Sci.* **2021**, *548*, 149269. [CrossRef]
38. Nupriyonok, I.S.; Chaplanov, A.M.; Shibko, A.N. Oxidation of titanium films irradiated with weak photon beam in the course of thermal treatment. In Proceedings of the 5th International Conference on Industrial Lasers and Laser Applications' 95: International Society for Optics and Photonics, Moscow, Russia, 24–26 June 1995; Volume 2713, pp. 321–324.
39. Zhou, B.; Jiang, X.; Liu, Z.; Shen, R.; Rogachev, A.V. Preparation and characterization of TiO_2 thin film by thermal oxidation of sputtered Ti film. *Mater. Sci. Semicond. Process.* **2013**, *16*, 513–519. [CrossRef]
40. Yeh, M.-Y.; Lee, P.-Y.; Shang, J.-T.; Lee, Y.-C. Effect of thermal oxidation temperatures on the phase evolution and photocatalytic property of tungsten-doped TiO_2 thin film. *Jpn. J. Appl. Phys.* **2018**, *57*, 125801. [CrossRef]
41. Pouilleau, J.; Devilliers, D.; Garrido, F.; Durand-Vidal, S.; Mahé, E. Structure and composition of passive titanium oxide films. *Mater. Sci. Eng. B* **1997**, *47*, 235–243. [CrossRef]
42. Stegemann, C.; Moraes, R.S.; Duarte, D.A.; Massi, M. Thermal annealing effect on nitrogen-doped TiO_2 thin films grown by high power impulse magnetron sputtering plasma power source. *Thin Solid Films* **2017**, *625*, 49–55. [CrossRef]

43. Khan, H.; Bera, S.; Sarkar, S.; Jana, S. Fabrication, structural evaluation, optical and photoelectrochemical properties of soft lithography based 1D/2D surface patterned indium titanium oxide sol-gel thin film. *Surf. Coat. Technol.* **2017**, *328*, 410–419. [CrossRef]
44. Abdullah, S.A.; Sahdan, M.Z.; Nayan, N.; Embong, Z.; Hak, C.R.C.; Adriyanto, F. Neutron beam interaction with rutile TiO_2 single crystal (111): Raman and XPS study on Ti^{3+}-oxygen vacancy formation. *Mater. Lett.* **2020**, *263*, 127143. [CrossRef]
45. Nair, P.B.; Justinvictor, V.B.; Daniel, G.P.; Joy, K.; Ramakrishnan, V.; Thomas, P. V Effect of RF power and sputtering pressure on the structural and optical properties of TiO_2 thin films prepared by RF magnetron sputtering. *Appl. Surf. Sci.* **2011**, *257*, 10869–10875. [CrossRef]
46. Kunti, A.K.; Sekhar, K.C.; Pereira, M.; Gomes, M.J.M.; Sharma, S.K. Oxygen partial pressure induced effects on the microstructure and the luminescence properties of pulsed laser deposited TiO_2 thin films. *AIP Adv.* **2017**, *7*, 15021. [CrossRef]
47. Takahashi, K.; Yoshikawa, A.S. *Fundamental Properties and Modern Photonic and Electronic Devices*; Springer: New York, NY, USA, 2007.
48. Bikondoa, O.; Pang, C.L.; Ithnin, R.; Muryn, C.A.; Onishi, H.; Thornton, G. Direct visualization of defect-mediated dissociation of water on TiO_2 (110). *Nat. Mater.* **2006**, *5*, 189–192. [CrossRef]
49. Minato, T.; Sainoo, Y.; Kim, Y.; Kato, H.S.; Aika, K.; Kawai, M.; Zhao, J.; Petek, H.; Huang, T.; He, W. The electronic structure of oxygen atom vacancy and hydroxyl impurity defects on titanium dioxide (110) surface. *J. Chem. Phys.* **2009**, *130*, 124502. [CrossRef]
50. Shi, H.; Liu, Y.-C.; Zhao, Z.-J.; Miao, M.; Wu, T.; Wang, Q. Reactivity of the defective rutile TiO_2 (110) surfaces with two bridging-oxygen vacancies: Water molecule as a probe. *J. Phys. Chem. C* **2014**, *118*, 20257–20263. [CrossRef]
51. Obregón, S.; Rodríguez-González, V. Photocatalytic TiO_2 thin films and coatings prepared by sol–gel processing: A brief review. *J. Sol-Gel Sci. Technol.* **2021**, *58*, 1–17. [CrossRef]
52. Qutub, N.; Pirzada, B.M.; Umar, K.; Sabir, S. Synthesis of CdS nanoparticles using different sulfide ion precursors: Formation mechanism and photocatalytic degradation of Acid Blue-29. *J. Environ. Chem. Eng.* **2016**, *4*, 808–817. [CrossRef]
53. Yu, J.C.; Zhang, L.; Zheng, Z.; Zhao, J. Synthesis and characterization of phosphated mesoporous titanium dioxide with high photocatalytic activity. *Chem. Mater.* **2003**, *15*, 2280–2286. [CrossRef]
54. Pan, X.; Yang, M.-Q.; Fu, X.; Zhang, N.; Xu, Y.-J. Defective TiO_2 with oxygen vacancies: Synthesis, properties and photocatalytic applications. *Nanoscale* **2013**, *5*, 3601–3614. [CrossRef]
55. Stojadinović, S.; Tadić, N.; Radić, N.; Grbić, B.; Vasilić, R. Effect of Tb^{3+} doping on the photocatalytic activity of TiO_2 coatings formed by plasma electrolytic oxidation of titanium. *Surf. Coatings Technol.* **2018**, *337*, 279–289. [CrossRef]
56. Sunada, K.; Watanabe, T.; Hashimoto, K. Studies on photokilling of bacteria on TiO_2 thin film. *J. Photochem. Photobiol. A Chem.* **2003**, *156*, 227–233. [CrossRef]
57. Dasari, T.P.; Pathakoti, K.; Hwang, H.-M. Determination of the mechanism of photoinduced toxicity of selected metal oxide nanoparticles (ZnO, CuO, Co_3O_4 and TiO_2) to *E. coli* bacteria. *J. Environ. Sci.* **2013**, *25*, 882–888. [CrossRef]
58. Kubacka, A.; Diez, M.S.; Rojo, D.; Bargiela, R.; Ciordia, S.; Zapico, I.; Albar, J.P.; Barbas, C.; dos Santos, V.A.P.M.; Fernández-García, M. Understanding the antimicrobial mechanism of TiO_2-based nanocomposite films in a pathogenic bacterium. *Sci. Rep.* **2014**, *4*, 1–9. [CrossRef]
59. Van Acker, H.; Coenye, T. The role of reactive oxygen species in antibiotic-mediated killing of bacteria. *Trends Microbiol.* **2017**, *25*, 456–466. [CrossRef]
60. Pant, B.; Park, M.; Park, S.-J. Recent advances in TiO_2 films prepared by sol-gel methods for photocatalytic degradation of organic pollutants and antibacterial activities. *Coatings* **2019**, *9*, 613. [CrossRef]
61. Phuinthiang, P.; Trinh, D.T.T.; Channei, D.; Ratananikom, K.; Sirilak, S.; Khanitchaidecha, W.; Nakaruk, A. Novel strategy for the development of antibacterial TiO_2 thin film onto polymer substrate at room temperature. *Nanomaterials* **2021**, *11*, 1493. [CrossRef]
62. Russell, A.D. Similarities and differences in the responses of microorganisms to biocides. *J. Antimicrob. Chemother.* **2003**, *52*, 750–763. [CrossRef]
63. Epand, R.M.; Epand, R.F. Lipid domains in bacterial membranes and the action of antimicrobial agents. *Biochim. Biophys. Acta (BBA) Biomembranes* **2009**, *1788*, 289–294. [CrossRef]
64. Vyas, S.; Tiwary, R.; Shubham, K.; Chakrabarti, P. Study the target effect on the structural, surface and optical properties of TiO_2 thin film fabricated by RF sputtering method. *Superlattices Microstruct.* **2015**, *80*, 215–221. [CrossRef]
65. Tauc, J. Optical Properties and Electronic Structure of Amorphous Semiconductors. In *Optical Properties of Solids*; Springer: Berlin/Heidelberg, Germany, 1969; pp. 123–136.
66. Tayade, R.J.; Natarajan, T.S.; Bajaj, H.C. Photocatalytic degradation of methylene blue dye using ultraviolet light emitting diodes. *Ind. Eng. Chem. Res.* **2009**, *48*, 10262–10267. [CrossRef]
67. Espitia, P.J.P.; de Soares, N.F.F.; dos Reis Coimbra, J.S.; de Andrade, N.J.; Cruz, R.S.; Medeiros, E.A.A. Zinc oxide nanoparticles: Synthesis, antimicrobial activity and food packaging applications. *Food Bioprocess Technol.* **2012**, *5*, 1447–1464. [CrossRef]